

Topographic control of asynchronous glacial advances: A case study from Annapurna, Nepal

Beth Pratt-Sitaula,¹ Douglas W. Burbank,² Arjun M. Heimsath,³ Neil F. Humphrey,⁴ Michael Oskin,⁵ and Jaakko Putkonen⁶

Received 9 October 2011; revised 15 November 2011; accepted 18 November 2011; published 30 December 2011.

[1] Differences in the timing of glacial advances, which are commonly attributed to climatic changes, can be due to variations in valley topography. Cosmogenic ¹⁰Be dates from 24 glacial moraine boulders in 5 valleys define two age populations, late-glacial and early Holocene. Moraine ages correlate with paleoglacier valley hypsometries. Moraines in valleys with lower maximum altitudes date to the late-glacial, whereas those in valleys with higher maximum altitudes are early Holocene. Two valleys with similar equilibrium-line altitudes (ELAs), but contrasting ages, are <5 km apart and share the same aspect, such that spatial differences in climate can be excluded. A glacial mass-balance cellular automata model of these two neighboring valleys predicts that change from a cooler-drier to warmer-wetter climate (as at the Holocene onset) would lead to the glacier in the higher altitude catchment advancing, while the lower one retreats or disappears, even though the ELA only shifted by ~120 m. **Citation:** Pratt-Sitaula, B., D. W. Burbank, A. M. Heimsath, N. F. Humphrey, M. Oskin, and J. Putkonen (2011), Topographic control of asynchronous glacial advances: A case study from Annapurna, Nepal, *Geophys. Res. Lett.*, 38, L24502, doi:10.1029/2011GL049940.

1. Introduction

[2] Glaciers are potentially valuable recorders of terrestrial climate change – delicately tuned to the combined effect of snow fall and temperature. The complex reality of glacial behavior, however, can hinder efforts to create reliable climatic reconstructions. Although regional climatic signals are commonly discernible, individual glaciers have been shown to advance and retreat asynchronously at local, regional, and global scales [e.g., *Benn and Owen, 1998; Gillespie and Molnar, 1995*]. Further understanding of the factors that lead to disparate glacial behavior will improve interpretation of past climate and prediction of future glacial change. Previous researchers have suggested that hypsometry plays a

role in glacial asynchrony [e.g., *Chenet et al., 2010; Kerr, 1993*], but this study is the first to test the hypothesis rigorously with a combination of modeling and field work. Results from this study quantify, more thoroughly than in previous studies, how glacial hypsometry, as well as climate, can drive asynchronous glacial behavior.

2. Background and Methods

[3] Prior studies of glaciation in the Annapurna area are limited to broad regional surveys [e.g., *Fort and Derbyshire, 1988; Hagen, 1968; Owen et al., 1998*], recent glacial erosion estimates [*Heimsath and McGlynn, 2008*], and limited, scattered ¹⁰Be dating [*Zech et al., 2009*]. Further east in Nepal, other glacial dating studies [*Finkel et al., 2003; Gayer et al., 2006; Owen et al., 2009*] have found ice extent maxima at times broadly consistent with those presented here. This study in the Annapurna region of central Nepal (Figure 1) combines field observations, ¹⁰Be dating of glacial boulders, digital elevation model (DEM) analysis, and cellular automata modeling of glacial mass balance to test the hypothesis that identical climate change can cause coeval advance and retreat of neighboring glaciers in drainage basins that have significantly different hypsometries.

2.1. Cosmogenic ¹⁰Be Dating

[4] We dated moraines in valleys spanning a range of locations and altitudinal extents. Two valleys lie north (leeward) of the Annapurna Range (Figure 1b); one is on the range crest (Figure 1c); and two lie to the south (windward) (Figure 1d). Syaktan valley (Figure 1b) and Danfe valley (Figure 1d) descend from peaks ≥5500 m, whereas ridgelines in the other 3 valleys are <5200 m high. The dated glacial valleys are small (<8 km²) and not complicated by significant avalanching which can displace snow far below the climatic equilibrium [*Harper and Humphrey, 2003*]. Valley bottoms are free of obvious hummocky morphology and lack large headwalls, suggesting that the glacier surfaces were free of extensive debris cover. Each valley has only one major set of preserved moraines and no modern glaciers. The moraines have multiple crests in places, but soil development and morphology do not change significantly from one crest to the next, thereby suggesting deposition over a short interval. Of particular note, the two northern valleys (Figure 1b) lie <5 km apart and have the same aspect and climate. Four to seven moraine-crest boulders were sampled from each valley (Figure 1 and Table S1 in the auxiliary material).¹ We prepared samples using standard procedures

¹Geological Sciences Department, Central Washington University, Ellensburg, Washington, USA.

²Department of Earth Science, University of California, Santa Barbara, California, USA.

³School of Earth and Space Exploration, Arizona State University, Tempe, Arizona, USA.

⁴Department of Geology and Geophysics, University of Wyoming, Laramie, Wyoming, USA.

⁵Geology Department, University of California, Davis, California, USA.

⁶Department of Geology and Geological Engineering, University of North Dakota, Grand Forks, North Dakota, USA.

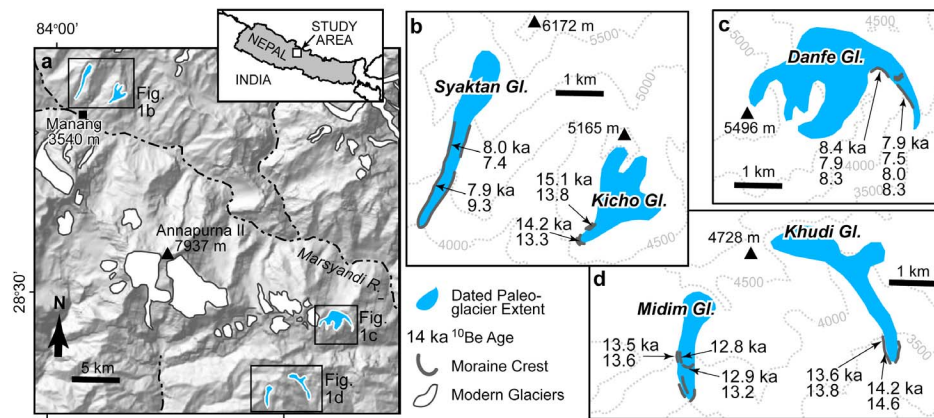


Figure 1. a) Shaded relief map of the field area with locations of detailed maps. Main Marsyandi valley contains numerous degraded, pre-Holocene glacial and landslide deposits more fully described in regional surveys [Fort and Derbyshire, 1988; Hagen, 1968; Owen *et al.*, 1998]. b–d) Detailed maps of sample locations, ^{10}Be exposure ages, moraine crests, and paleoglacier extents.

[e.g., Kohl and Nishiizumi, 1992] and measured the ^{10}Be concentrations at Lawrence Livermore National Laboratory. Ages were calculated using v2.2 CRONUS-Earth online calculator [Balco *et al.*, 2008]. Ages presented in this paper are from the Lal [1991] and Stone [2000] time-dependent scaling model. Results from other scaling models (Table S2) nearly all fall within the external error bars of the time-dependent Lal/Stone model (Figure 2a), thus differences in scaling models, although important to consider, do not affect the conclusions of the study.

2.2. Topographic Analysis: Glacial Hypsometry and Equilibrium Line Altitudes

[5] Based on valley morphology and moraine location determined from air photo and field analysis, we digitized areas for each paleoglacier onto georeferenced topographic maps [Finnish Meteorological Institute, 2001], and glacier-bed hypsometry was calculated from a 3-arcsecond ($\sim 90\text{-m}$) Shuttle Radar Topography Mission data (Figure 3). For each paleoglacier, the former ELA (equilibrium-line altitude where net snow mass input is balanced by the local net snow melt) was estimated using the calculated hypsometries and assuming an accumulation-area ratio of 0.60. Work in Nepal [Ageta and Higuchi, 1984; Benn and Lehmkuhl, 2000] and elsewhere [e.g., Benn *et al.*, 2005; Porter, 2000] shows that the accumulation zone typically occupies 50–80% of a glacier's area. Because use of other accumulation-area ratios [e.g., Kern and Laszlo, 2010] or other methods (e.g., area-altitude balance ratio [Benn *et al.*, 2005; Rea, 2009]) changes the absolute ELA estimates somewhat, but does not alter our primary conclusions, we used a method and ratio in common use for inter-study comparability.

2.3. Glacial Mass Balance Model

[6] A cellular automata model [Harper and Humphrey, 2003] was used to investigate how changes in glacial ELA and mass balance influence glacial dynamics. The model requires an input ELA, a mass-balance curve (change in mass gain or loss versus altitude), and topography of the entire glacial valley. From these, the net mass of snow input is calculated for each altitude. At each time-step, the ice is

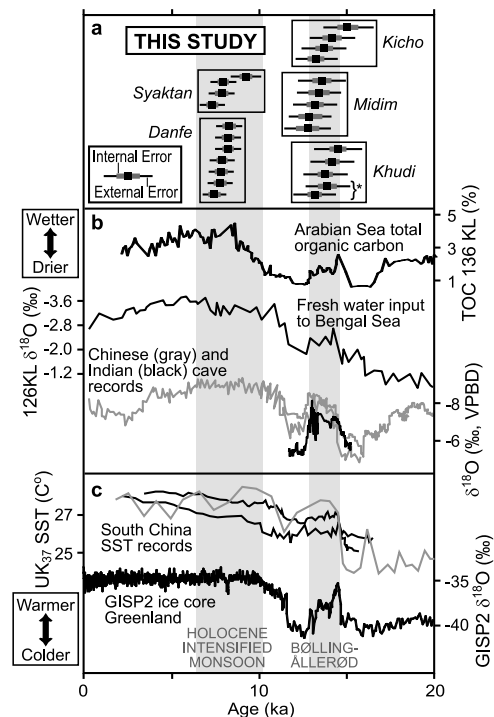


Figure 2. Glacial chronologies and paleoclimate proxies. Vertical gray bands indicate the temporal extent of the Holocene intensified monsoon and the Bølling-Ållerød. a) Moraine boulder ^{10}Be exposure ages from this study. Names and boxes refer to individual valleys (see Figure 1). The gray error bar shows the internal error from laboratory, AMS, and snow-shielding uncertainties. The thin black error bar shows the external error from the production rate scaling model. *Indicates single sample that was split for analysis and provides a measure of laboratory repeatability. b) Paleoprecipitation proxies: Arabian Sea total organic carbon [Schulz *et al.*, 1998], Bengal Sea freshwater [Kudrass *et al.*, 2001], Hulu [Wang *et al.*, 2001] and Dongge [Yuan *et al.*, 2004] cave records in gray, Tinta cave record [Sinha *et al.*, 2005] in black. c) Paleotemperature proxies: South China Sea surface temperatures (SST) in black [Kienast *et al.*, 2001] and gray [Oppo and Sun, 2005] and GISP2 ice core record [Alley *et al.*, 1995].

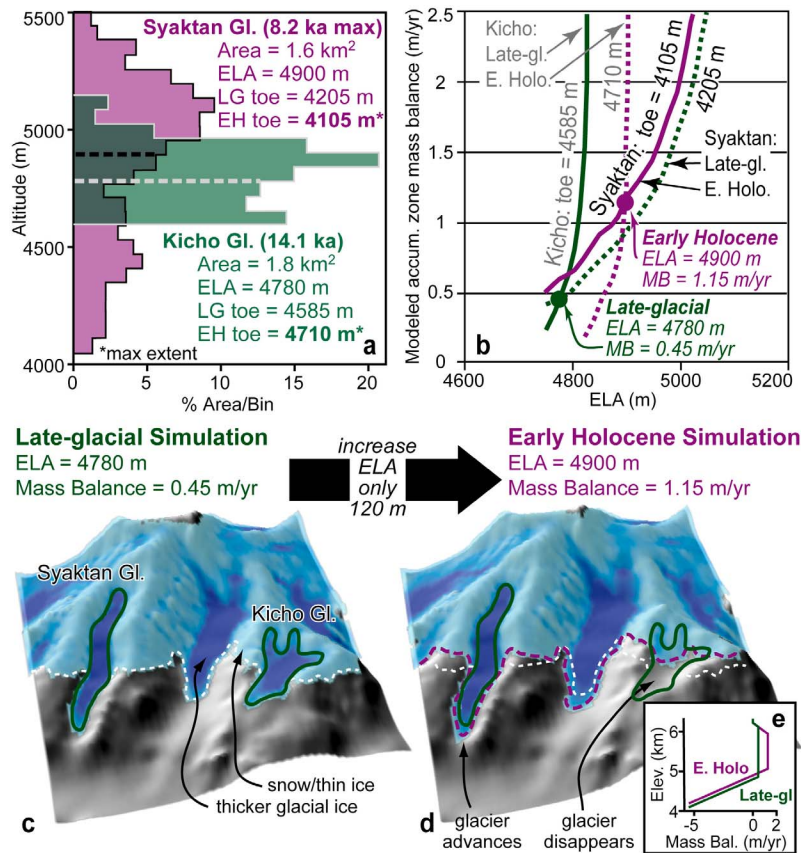


Figure 3. Topographic analysis and cellular automata model results. a) ELAs and glacial bed hypsometries of the paleoglaciers in Syktan and Kicho valleys, early Holocene (EH) and late-glacial (LG) chronozone, respectively. b) Model-derived relationship between ELA and accumulation-zone mass balance (AZMB). Green indicates late-glacial model, and purple is early Holocene. Solid lines show relationship when modeled glaciers are at their mapped toe elevations. At the topographically estimated ELA of 4780 m for the maximum Kicho glacier, the model predicts Kicho's AZMB = 0.45 m/yr. This AZMB places Syktan's toe at 4205 m (dashed green line), 100 m higher than its observed maximum extent. Similarly, at ELA = 4900 m, Syktan reaches full extent when the AZMB = 1.15 m/yr, but Kicho's toe elevation rises to 4710 m (dashed purple line), which is so high the glacier probably does not exist anymore. c) Late-glacial simulation: both valleys are predicted to have had robust glaciers. d) Early Holocene simulation: raising the ELA just 120 m causes the Kicho Gl. to recede significantly, whereas the Syktan Gl. advances if the mass balance is increased. e) Mass balance curves used. Balance gradient in ablation zone = 8 m/yr/km [Harper and Humphrey, 2003].

routed across the landscape according to two basic assumptions about ice behavior. If the surface slope is $>35^\circ$, it is unstable and any snow avalanches to the next lowest cell. If the ice surface is $<35^\circ$, the ice thickness varies in order to maintain a basal shear stress (τ_b) of 1 bar [Nye, 1952; Paterson, 1994]. Thus,

$$\tau_b = \rho g h S \approx 1 \text{ bar}, \quad (1)$$

where ρ = density, g = force due to gravity, h = ice thickness, and S = ice surface slope. Any ice thickness causing stresses exceeding 1 bar will flow to the lowest adjacent cell. To match the values determined for modern Annapurna area glaciers [Harper and Humphrey, 2003], the upper boundary for significant snowfall was set to 6200 m, the mass balance was set to be constant through the accumulation area until just above the ELA, where it decreases at a constant rate of 8 m/yr per km of altitude through the ablation area. The bulk of the studied glacial valleys are below 6000 m, such that

model results are insensitive to the upper snow boundary. Likewise, changing the mass balance gradient in the ablation zone by ± 4 m/yr/km does not significantly change the outcome. Although the model does not mimic ice flow exactly, it succeeds in predicting general ice extent in modern Himalayan glaciers [Harper and Humphrey, 2003].

3. Results and Interpretation

[7] The ^{10}Be exposure ages were consistent within each valley (Table 1 and Figure 2a), with no outliers. The dates fall into 2 distinct populations: 15–13 ka and ~ 8 ka. Kicho valley ages range from 13.3 to 15.1 ka with a sample mean of 14.1 ± 0.8 ka, Midim valley ages are 12.8–13.6 ka with a mean of 13.3 ± 0.3 ka, and Khudi valley ages are 13.2–14.6 ka with a mean of 14.1 ± 0.4 ka. The younger ages come from Syktan valley with a range of 7.4–9.3 ka with a mean of 8.2 ± 0.8 ka and Danfe valley where ages are 7.5–8.3 ka with a mean of 8.0 ± 0.3 ka. We conclude that spatially

